Eur. Phys. J. D **8**, 227–239 (2000)

THE EUROPEAN PHYSICAL JOURNAL D

EDP Sciences

Energy transfer studies in krypton-xenon mixtures excited in a cooled DC discharge

B. Krylov[1], G. Gerasimov[1], A. Morozov[2], A. Arnesen[2], R. Hallin[2,a], and F. Heijkenskjold[2]

[1] Vavilov State Optical Institute, Birzhevaja Line 12, St. Petersburg, 199034 Russia
[2] Uppsala University, Department of Physics, Box 530, 751 21 Uppsala, Sweden

Received 12 May 1999 and Received in final form 27 August 1999

Abstract. The VUV spectrum of gaseous mixtures of krypton with a small amount of xenon added was investigated in the range 115–200 nm. The mixtures were excited in a capillary DC discharge where the capillary could be cooled by using liquid nitrogen. The mixed molecule band around the Xe I resonance line at $\lambda = 147$ nm and the mixed molecule continuum to the long wavelength side from the line were analysed. The band around $\lambda = 147$ nm was identified as transitions between a weakly bound excited state and the weakly bound ground state of XeKr molecules. When cooling the capillary wall, the appearance of the Xe_2 continuum was observed. The effect is ascribed to energy transfer between molecular states as a consequence of radiation trapping in the band around $\lambda = 147$ nm. The role of the mixed molecule in the formation of the VUV spectrum of the gas mixture is discussed and underlined.

PACS. 33.20.Ni Vacuum ultraviolet spectra – 33.50.Hv Radiationless transitions, quenching

Introduction

The main part of the research on rare-gas excimers has been centered around the homonuclear species Ar_2^*, Kr_2^* and Xe_2^* and the interest in the VUV fluorescence of rare gases is to a large extent connected with the development of VUV light sources, including lasers. Not so many publications are devoted to the excitation processes and optical spectra of heteronuclear rare-gas excimers like the XeKr molecule.

The lowest excited states of the Xe*Kr molecules are built up by the same Xe atomic states, *i.e.* the resonant $^3P_1$ and the metastable $^3P_2$ states, as the lowest excited states of the Xe_2^* molecule (Fig. 1). Therefore transitions from excited states of XeKr and Xe_2 to the weakly bound ground states give overlapping VUV continua. This is the reason why the identification of the XeKr molecule spectrum was a debated topic in many previous studies.

Like the spectra of other rare gas mixtures, the Xe–Kr VUV spectrum is intriguing because of the manifestation of energy transfer processes between the rare gases (from a light gas to a heavier one). The authors of [1,2] studied, among others, gaseous krypton-xenon mixtures excited with a pulsed electric discharge (70–640 torr total pressure, 0.001–0.1% of xenon) [1] and with an α-source (1000 torr total pressure, 0.0025–2.5% of xenon) [2]. They reported that small amounts of another rare gas admixture, *e.g.* Xe in Kr, acted as a very efficient electronic energy acceptor. This led to a gradual disappearance

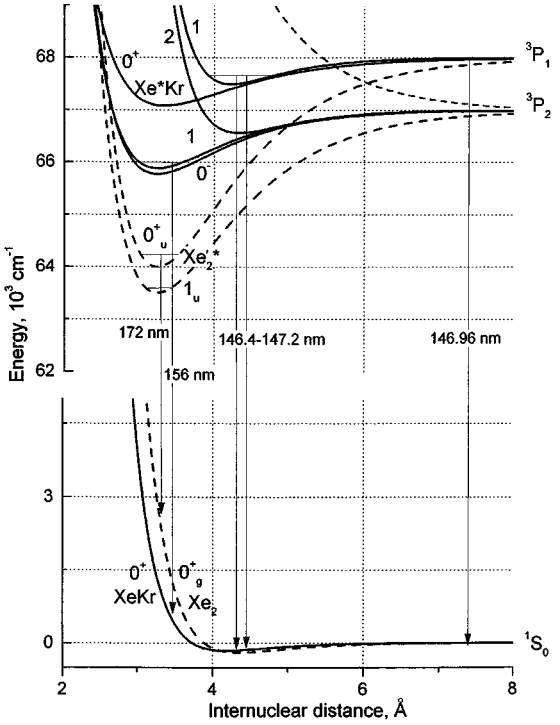

Fig. 1. Morse potential curves for the lowest XeKr and Xe_2 (dashed curves) electronic states. Potential curve parameters and references are listed in Table 1. See also comments in Section 3. The main optical transitions discussed in the work are indicated.

[a] e-mail: reinhold.hallin@fysik.uu.se

of the molecular continuum of the host gas and to the appearance of the resonance atomic line and the molecular continuum of the admixture. The relative contributions of two energy transfer mechanisms involving atom-atom and molecule-atom energy transfer were estimated. The authors [1,2] underlined that molecule-atom energy transfer is a resonant process for a wide range of excitation energies and that this process is characterised by a large ($\sim 10^{-14}$ cm^2) cross section.

Also, a spectroscopic study of krypton-xenon mixtures with α-particle excitation [3] (total pressure 100–500 torr, 0.001–10% of xenon) verified that energy transfer from krypton atoms and molecules to xenon is very efficient. The spectra of mixtures with only a few percent of xenon were very similar in shape and intensity to those of pure xenon. In contrast to [1,2], where the reaction constants were obtained from measurements of spectral intensity ratios, reaction rates and a kinetic scheme of the transfer phenomena were determined from measurements of the time constants governing the decay of the main krypton and xenon emissions in the VUV.

Many additional details of the kinetic scheme of the energy transfer processes, including reaction rates, were obtained with pulsed electron-beam excitation and time-of-flight techniques in the publications [4,5] (total pressure 25–900 torr, 0.1–10% of xenon, time-dependent and time-independent measurements). In particular, the transfer rates to the excited mixed molecule $(KrXe)^*$ were obtained.

The results of the recent work [6] obtained with a pulsed discharge excitation (total pressure 5–140 torr, 0.4–50% of xenon), have elucidated the nature and the position of the emission maximum in the region of 156 nm. It is definitely ascribed to transitions in the Xe^*Kr molecule as the analogy of the second continuum of homonuclear inert-gas molecules. The relaxation constants of Xe^*Kr and Xe_2^* molecules with Kr as buffer gas were estimated and found to have similar values for both excimer systems.

Interesting results were also obtained when excimers formed in aggregates of condensed phases were investigated [7–10]. For example, in [8] solid layers of Kr were bombarded with thermal Xe atoms in the metastable $^3P_2$ state. From the observed VUV emission, the potential parameters for the $Xe(^3P_2) + Kr(^1S_0)$ excimer system were deduced.

Semiempirical calculations of the $Xe(^3P_1, ^3P_2)$–$Kr(^1S_0)$ interaction potentials, the radiative lifetimes of the XeKr lower excited states and the VUV spectra of the heteronuclear molecules were performed in [11–13].

Part of the cited works also contains a considerable amount of data about other inert gas mixtures (xenon-argon, krypton-argon and others) which might be useful for understanding krypton-xenon spectra.

In this paper we present spectra of krypton-xenon mixtures obtained in uncooled and cooled capillary DC discharges. The spectra show that the role of mixed XeKr molecules has not been adequately taken into account in the previous publications. Intense formation of excited XeKr molecules begins at very low partial densities of xenon and takes place in a xenon concentration range up to more than 1%. These molecules were often not included in the kinetic models or were included only passively as a final emitting product. We have tried to analyse carefully the participation of the mixed molecules in the energy transfer processes. The result forces us to consider the mixed molecules as a necessary component of the kinetic models.

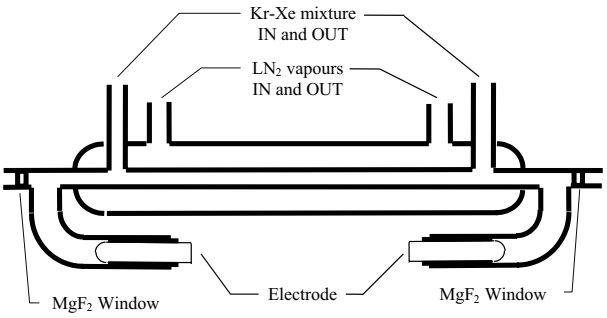

Fig. 2. Scheme of the gas discharge tube used for the experiments.

Furthermore, the spectra recorded at relatively high both total and partial xenon pressures have demonstrated that the spectral intensity distribution depends strongly on the gas temperature.

1 Experiment

Spectra have been recorded in the range 115–200 nm from a DC capillary discharge at total gas pressures of 30–300 torr and with 0.01–1% xenon admixture to the krypton gas. The gas inside the capillary could be cooled down to the temperature of condensation.

The discharge tube (see Fig. 2) was made of fused silica with windows of magnesium fluoride to allow detection of the VUV spectrum down to 115 nm. Two cold tungsten electrodes were melted into side branches of the tube. The DC discharge (10–50 mA) took place in a capillary tube of 0.30 m length and 1.5 mm inner diameter and the tube was connected to a vacuum system to be evacuated and filled with gas. An initial pressure of less than 2×10^{-7} torr was achieved before filling the system. The distance between the magnesium fluoride windows and the capillary ends could be changed but was usually about 10 mm.

It is a well-known phenomenon for a DC discharge in a gas mixture that the gas can be separated by the running discharge so that one of the gaseous components is collected near the anode while the other component gathers around the cathode. To prevent this separation, a flow of the gas mixture through the capillary was maintained with a specially designed fan.

The capillary was surrounded by a concentric tube also made of fused silica. The volume inside this tube was flushed with cold nitrogen vapour in order to cool the capillary walls. The capillary wall temperature was adjusted by changing the inlet pressure of the vapours and measured with a copper-constantan thermocouple within the

range 100–400 K. To prevent unnecessary evaporation of liquid nitrogen, the outer wall was thermally isolated.

Krypton-xenon mixtures were prepared in a special volume, connected to high pressure gas bottles containing high purity krypton and krypton-xenon mixtures (1% and 0.1% of Xe). It took about one hour to prepare a homogeneous gas mixture.

The spectra were recorded using a 1 m normal-incidence vacuum spectrometer with 0.417 nm/mm dispersion. The spectral resolution, determined by the widths of the entrance and exit slits, was 0.015 nm. A pm-tube with a magnesium fluoride window and a cesium-tellurium photocathode, operating in the photon counting mode, was used as detector. The photon counting time per channel was in the range 0.1–0.5 s and the peak count rate reached 8×10^4 counts per second. The main part of the wavelength region 115 to 200 nm was usually recorded with 640 channels per spectrum, *i.e.* with a recording system spectral resolution of 0.125 nm. However, several narrow spectral ranges, including in particular the atomic lines of xenon and krypton and lines of impurities, were usually recorded with higher spectral resolution, down to 0.02 nm or better. No corrections for changes in window transmission, grating efficiency and detector efficiency within the investigated wavelength range have been made for the spectra shown in this article.

The krypton, xenon and krypton-xenon molecular continua and the resonance lines of atomic krypton (λ_1 = 116.487 nm, λ_2 = 123.584 nm) and xenon (λ_3 = 129.559 nm, $\lambda_4 = 146.961$ nm) were observed in the spectra. Besides, the resonance line of impurity hydrogen (λ = 121.567 nm) and groups of carbon lines ($\lambda_1 = 156.1$ nm, $\lambda_2 = 165.7$ nm) were observed. The intensities of the impurity lines decreased as the discharge was cooled. We also examined the effect of the impurities on the intensities of the continua. According to our observations, a change of intensity caused by the impurities cannot have been more than a few percent after conditioning of the capillary tube.

2 Results of the experiment

When a small quantity of xenon (less than one percent of the total pressure) was added to krypton, the VUV emission spectrum changed in the same manner as in the above cited works, namely that the intensity of the krypton continuum decreased with increasing xenon partial pressure, and an intense peak of narrow-band radiation arose in the immediate vicinity of $\lambda = 147.0$ nm. Figure 3 illustrates the aforesaid: as an example, the spectra of pure krypton and krypton with an admixture of 0.1% of xenon are shown at a total pressure of 300 torr and a discharge current of 20 mA.

The narrow-band radiation at $\lambda = 147.0$ nm was in previous works completely ascribed to the atomic resonance line of xenon ($\lambda = 146.96$ nm). However, this identification is not correct in many cases. In reality, even at relatively low pressures of the "krypton-small amount of xenon" mixture, a structure of nonatomic origin appears

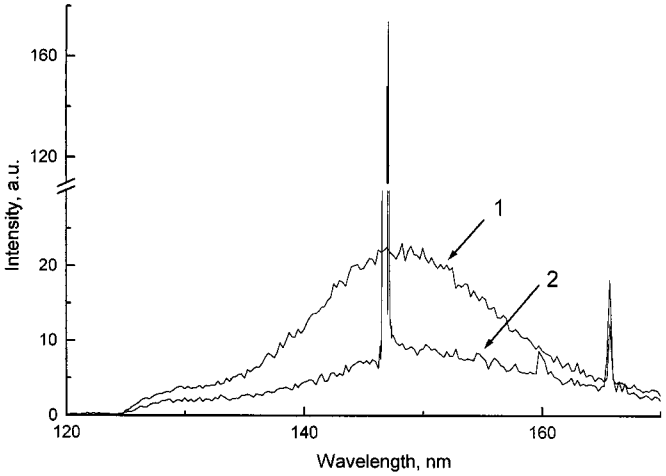

Fig. 3. Emission spectra from the capillary gas discharge showing the change of the spectral intensity distribution when a small quantity of xenon is added to krypton. 1 – pure krypton; 2 – krypton with an admixture of 0.1% of xenon. The total pressure was 300 torr and the discharge current 20 mA (no cooling).

near the xenon resonance line. Spectra of this mixture in the wavelength interval 146.5–147.3 nm, at the total pressure 30 torr and with different concentrations of xenon (0.05%, 0.25%, 1%), are shown in Figure 4. The figure demonstrates that at a concentration of xenon of 0.05%, corresponding to a partial pressure of 1.5×10^{-2} torr, the emission profile is already clearly asymmetric and a "shoulder" appears on the long wavelength side directly adjacent to the peak position of the atomic line which coincides with the peak of the absorption profile at higher xenon pressures. The shoulder is shifted from the atomic line by 0.06 nm. As the xenon concentration increases to 1% (0.30 torr), self-absorption becomes stronger and the upgrowing shoulder seems to be the main emission component. Also, with increasing xenon pressure, a relatively broad emission structure with several maxima, at least three, appears on the short wavelength side in the band 146.4–146.95 nm. This structure becomes more clearly defined at higher total pressures of the mixture, for example at the pressure 90 torr (Fig. 5).

If one compares the spectra in Figures 4 and 5, it is evident that the intensity of the atomic line and the components to the left and right of $\lambda = 146.96$ nm depend both on the partial pressure of xenon and on the total pressure of the mixture. The dependence on the krypton pressure is demonstrated more distinctly in Figure 6 where spectra recorded at the same xenon pressure of 0.15 torr and different total pressures (30, 60, and 300 torr) are presented.

Figures 4–6 also demonstrate the influence of self-absorption (in the emitting volume and in the gas layer between the discharge column and the exit window) on the spectrum. With increasing pressure, the absorption band becomes deeper and more asymmetric (wider to the long wavelength side) and the absorption profile seems

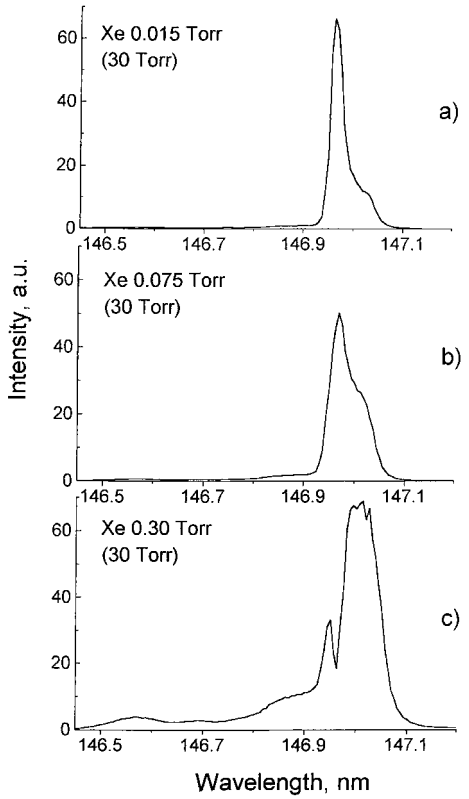

Fig. 4. Spectrum of narrow-band radiation of the krypton-xenon mixture near the xenon resonance line. The total pressure was 30 torr, the discharge current 20 mA and different concentrations of xenon: (a) 0.05%, (b) 0.25%, (c) 1%. The figure demonstrates that even at low pressures a structure of nonatomic origin appears near the xenon resonance line. The spectral resolution was 0.015 nm.

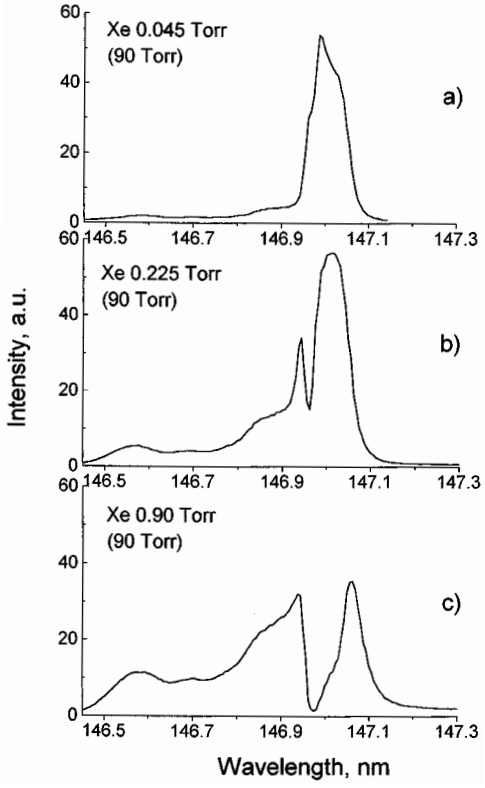

Fig. 5. Spectra of the krypton-xenon mixture near the xenon resonance line obtained at the total pressure 90 torr. The other specifications are the same as in Figure 4. The molecular structure is clearly defined. The influence of self-absorption on the spectrum in the vicinity of $\lambda = 147.0$ nm is distinctly seen.

to consist of two components (Fig. 5c), one appearing at the same wavelength as the emission "shoulder". The intensity of the absorption band depends both on the xenon pressure (Figs. 4 and 5) and on the krypton pressure (Fig. 6). The dependence on the krypton pressure indicates that the self-absorption also includes molecular absorption.

It should be pointed out that the emission peak at 147 nm in Figure 3 (spectrum 2) has a profile similar (actually, more self-absorbed) to the profile presented in Figure 6, spectrum 3. The total pressure in both cases is the same (300 torr), but the xenon partial pressure in Figure 3 is twice higher.

The influence of self-absorption on the emission spectrum is best shown in Figure 7a. Absorption maxima appear instead of emission maxima when the mixture Kr–Xe (0.25%) at 90 torr was replaced by the mixture Kr–Xe (1%) at 300 torr. Figure 7b shows densitometer traces of absorption spectra of Kr–Xe mixtures [14] (see also [15]) obtained at the xenon pressure 0.1 torr (all curves) and at the krypton pressures 6, 162, and 486 torr (curves 1, 2, and 3, respectively) in a 20 cm long cooled (160 K) absorption cell. It is evident from Figure 7 that the structure of the emission and absorption spectrum is the same: the peak positions in emission and absorption coincide

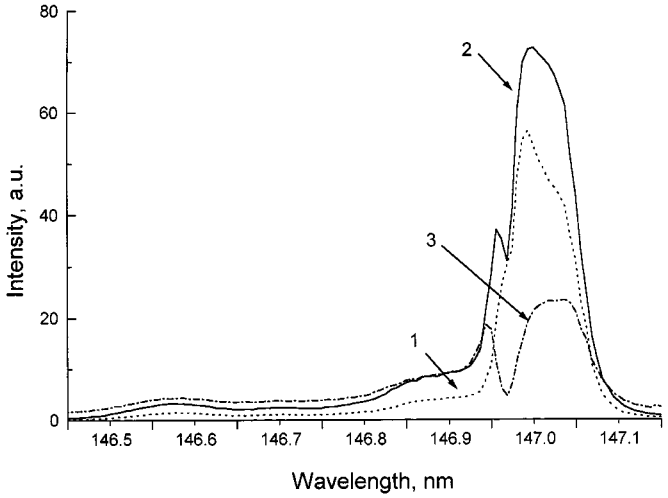

Fig. 6. The spectrum of the Kr–Xe mixture around $\lambda = 147.0$ nm and its dependence on the krypton pressure. The xenon pressure was constant, 0.15 torr. The total pressures were: (1) 30 torr; (2) 60 torr; (3) 300 torr. The discharge current was 20 mA. The spectral resolution was 0.015 nm.

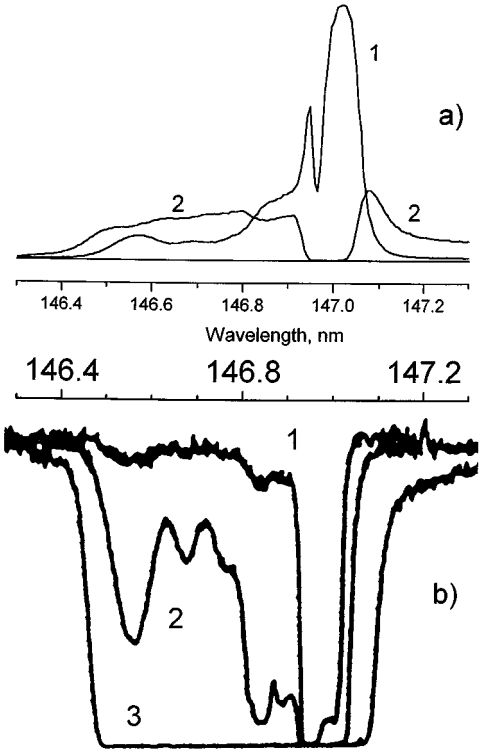

Fig. 7. Comparison of the emission (a) and absorption (b) spectrum of the krypton-xenon mixture around $\lambda = 147.0$ nm. The emission spectra (a) have been recorded at the total pressure 90 torr, 0.25% of Xe (curve 1) and 300 torr, 1% of Xe (curve 2). The absorption spectra (b) were recorded (densitometer traces are presented) in [14] at the xenon pressure 0.1 torr (all curves) and at the krypton pressures 6, 162, and 486 torr (curves 1, 2, and 3, respectively). As is evident, the structure of the emission spectrum and that of the absorption spectrum (peak positions, relative intensities and widths) is similar. See also specifications and comments in text.

precisely, and the relative intensities and widths are similar. The spectra obtained in [14] at high spectral resolution ($\sim$ 0.001 nm) showed that the resonance line is associated with two groups of discrete bands on its short wavelength side and with one group of bands on the long wavelength side (altogether more than 20 bands were observed). These bands appear as a result of bound-bound or bound-free transitions within the heteronuclear diatomic van der Waals molecules [14]. Figure 7 therefore allows identification of the emission spectra observed in the vicinity of $\lambda = 146.96$ nm on the basis of the results obtained in [14], namely: the xenon atomic line and bands of Xe*Kr molecules spanning the atomic line are seen, more or less self-absorbed by xenon atoms and mixed molecules.

The conclusion is that transitions in Xe*Kr molecules give a considerable contribution to the narrow-band radiation around $\lambda = 147.0$ nm that is crucial for the interpretation of the spectra. The identification of this band as well as the atomic xenon line and its use for measurements of molecule-atom energy transfer cross-sections therefore has to be done with care. It should be noted also that the appearance of the molecular structure in the range 146.40–146.95 nm is a good indicator that the strong molecular

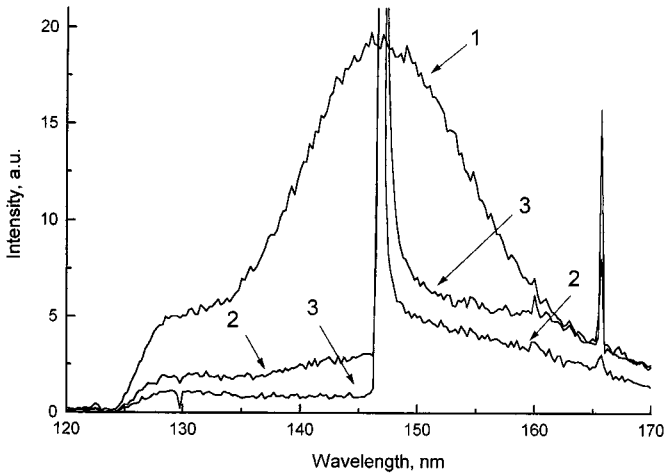

Fig. 8. Continua of krypton (curve 1) and krypton-xenon mixtures (curves 2 and 3). The total pressure was 300 torr (all curves), the Xe concentration 0.25% and 1.0% (curves 2 and 3, respectively). The continuous emission intensity in the mixture spectra is not equal on both sides of the band at 147.0 nm. The difference in intensities depends on the partial pressure of xenon. An explanation of the asymmetry is given in the text.

emission peak has arisen close to the xenon resonance line on the long wavelength side.

As can be seen in Figure 3 the krypton continuum goes down in intensity when xenon is added to krypton. However, the decrease in the intensity is not equal on both sides of the band at 147.0 nm: the long-wavelength side retains its intensity more than the short-wavelength side. The difference in intensities depends on the partial pressure of xenon (Fig. 8; total pressure 300 torr, 0.25% and 1.0% Xe). The short-wavelength continuum almost disappears when the mixture contains 1% (3 torr) of xenon. The explanation for the asymmetry is that an additional molecular continuum has appeared in the spectral region from the atomic line at 147.0 nm to approximately 190 nm. The extension of the continuum indicates that this is either the mixed molecule or the xenon molecule continuum. As was recently shown [6], each of these continua can appear as the dominant emission depending on the gas mixture. It was also verified in [6] that an emission maximum at $\lambda \approx 156$ nm is due to the mixed molecules and is an analogy of the krypton or xenon second continuum (see Fig. 1).

The maximum at 156 nm appeared in our spectra at "high" pressures of both krypton and xenon but was not clearly defined in spectra of the uncooled discharge (Fig. 9, spectrum 2; 300 torr, 1% Xe), and the maximum of the xenon second continuum was not seen. However, the spectrum changed completely when the capillary wall was cooled (Fig. 9, spectra 3 and 4). With decreasing wall temperature, an intense growth of the band at 156 nm was observed and, in addition, the xenon second continuum appeared and grew faster than the mixed molecule continuum (Fig. 9, spectrum 3). At a wall temperature close to the temperature of gas condensation, the second continuum from xenon molecules dominates the spectrum (Fig. 9, spectrum 4).

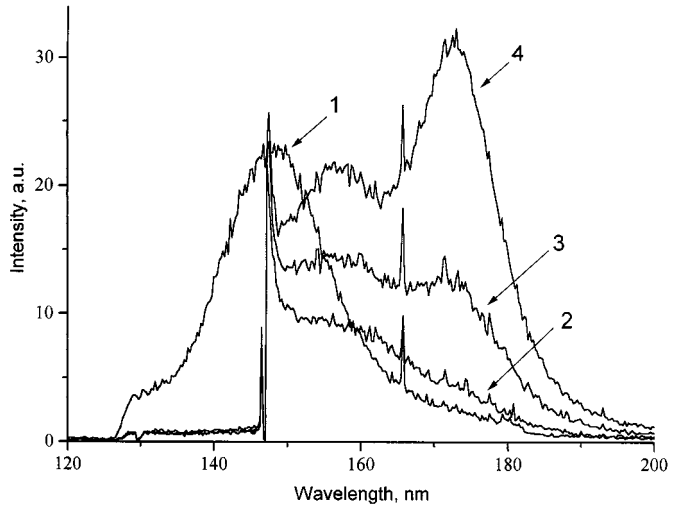

Fig. 9. Spectrum of a krypton-xenon mixture (curves 2–4) at the total pressure 300 torr, 1% of Xe, and its dependence on the gas temperature. The curves 2–4 show the change of the spectrum as a result of discharge capillary wall cooling from "no cooling" (curve 2) to a temperature close to the temperature of gas condensation (curve 4). With decreasing wall temperature, both the mixed molecule and the xenon continua grow, but the xenon continuum grows faster than the mixed molecule continuum (the atomic resonance line is self-absorbed more than in Fig. 8 because the distance between the discharge capillary and the exit window was longer than the usually used 10 mm). The krypton continuum (curve 1) is shown for comparison: the pressure was 300 torr, the discharge current 20 mA (without cooling).

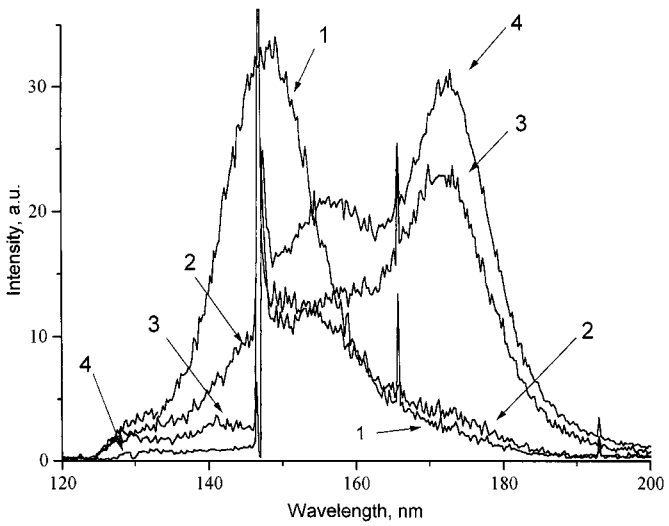

Fig. 10. Spectra of krypton (1) and krypton-xenon mixtures (2–4) at the lowest possible capillary wall temperature (close to the temperature of gas condensation). The curves (2–4) show how the intensities of the continua change with increasing xenon concentration: (1) 0%; (2) 0.1%; (3) 0.25%; (4) 1.0%. The total pressure was 300 torr, the discharge current 20 mA.

A similar growth of the mixed molecule and xenon continua was observed at room temperature in [2] (total pressure 1000 torr) and in [3] (total pressure 500 torr) when the xenon concentration was increased two orders of magnitude up to 2.5% and 1%, respectively.

Figure 10 exhibits the spectra of mixtures cooled close to the condensation temperature at 300 torr and different xenon concentrations (0.1%, 0.25%, 1%, spectra 2, 3 and 4 respectively). It is evident from the spectra that the growth of the band around 156 nm and, especially, the xenon second continuum occurs at relatively high xenon concentrations. A comparison of the krypton-xenon spectra 3 and 4 in Figure 10 with the spectrum of cooled (down to approximately the same temperature) krypton (spectrum 1) shows that, if we deal with energy transfer processes, they should be very effective.

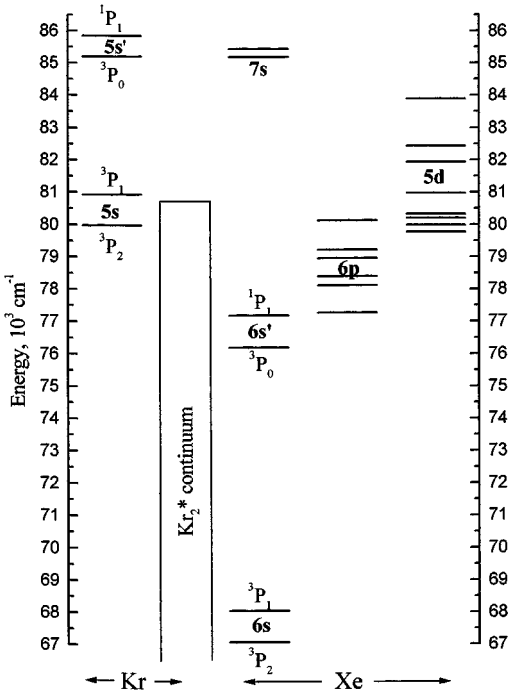

Fig. 11. Energy-level diagram for the lowest excited states of atomic krypton and xenon. The photon energy from the Kr_2^* continuum is also indicated.

3 Interpretation of the spectra and mechanisms of energy transfer

A simplified energy-level diagram for the lowest excited states of atomic Kr and nearby atomic Xe levels is shown in Figure 11.

Studies of electronic energy transfer processes in Kr–Xe mixtures were made in [1–5,16] using different methods for the excitation of the mixtures over a wide range of Kr host gas pressures and added Xe gas concentrations. Most of the results were obtained in time-resolved measurements from decay curves of atomic and molecular VUV emissions. We have tried to collect the most important processes for the discussion of our results and represent them in Figure 12. Reaction rates were taken from the previously cited works and also from [17–26,29,36].

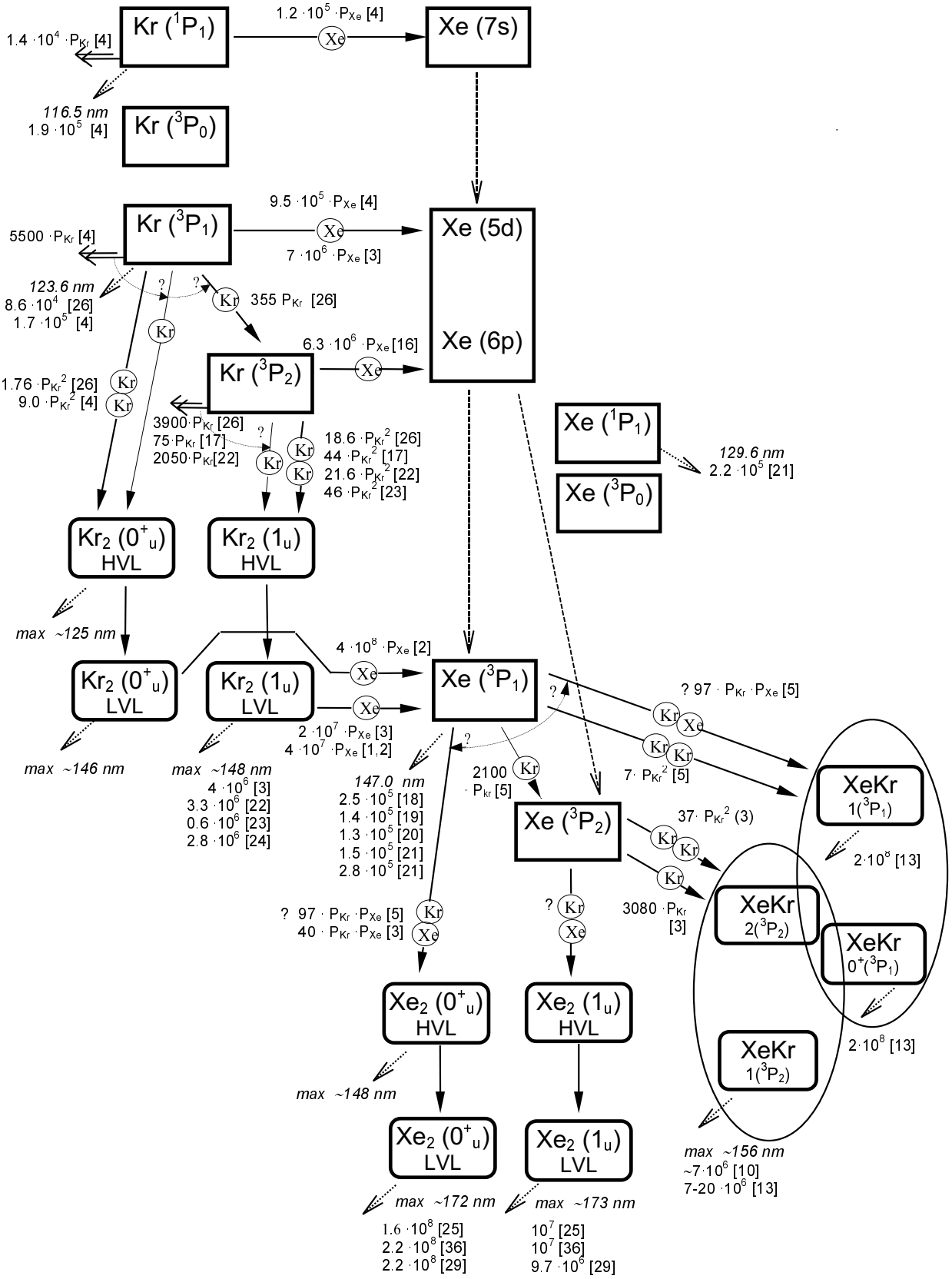

Fig. 12. Diagram of energy transfer processes in a "krypton-small amount of xenon" mixture, according to literature data. Reactions with a participation of electrons were not included. Rates are given in s^{-1}, $torr^{-1}s^{-1}$ and $torr^{-2}s^{-1}$. References are indicated to the publications listed at the end of the article. HVL (LVL) means high (low) vibrational levels. See also comments in Section 3.

However, some comments concerning the block diagram in Figure 12 should be made. Higher excited states of krypton atoms, not included in the diagram, have rather short ($10^{-7} - 10^{-8}$ s) radiative decay times, and therefore they can not act as efficient energy donors at low xenon concentrations. In contrast to the higher states, the lowest excited krypton states, included in the diagram, have rather long ($10^{-5} - 10^{-6}$ s) lifetimes since the optical transitions from the $^3P_0$ and $^3P_2$ levels are dipole forbidden or because of trapping of resonant radiation from the $^1P_1$ and $^3P_1$ states. The lifetime of trapped resonance radiation in krypton for atomic densities of 10^{16} cm^{-3} and higher is determined, according to [27,28], by the pressure broadening of the resonance line. Under such conditions, the decay constant $\beta(r)$ for a cylindrical tube with radius r is independent of the pressure and is given by $\beta(r) = (1/\tau_N)[0.205(\lambda/r)^{1/2}]$ [27,28], where τ_N is the natural lifetime of the upper state and λ is the wavelength of the resonance radiation. An experimental rate value of resonant radiation escape for the Kr($^1P_1$) state at $\lambda = 116.5$ nm, 1.9×10^5 s^{-1} ($r = 1$ cm) is given in [4] and two values are given for the Kr($^3P_1$) state at $\lambda = 123.6$ nm: 8.6×10^4 s^{-1} ($r = 5$ cm) [3,26] and 1.7×10^5 s^{-1} (r = 1 cm) [4].

A value of the quenching rate (that is, the constant of the reaction corresponding to the destruction of a Kr state by binary collisions with ground state Xe atoms) for the Kr($^1P_1$) resonant state has been found only in [4] (1.2×10^5 torr^{-1}s^{-1}); thus a comparison with other works is not possible. However, the quenching rate for the Kr($^3P_1$) resonant state, obtained from the Kr($^3P_1$) state decay curves (9.5×10^5 torr^{-1}s^{-1}) [4], can be compared with the result (7×10^6 torr^{-1}s^{-1}) deduced from the decay curves of the second krypton continuum at 145 nm [3]. The quenching rate of the Kr($^3P_2$) metastable state (6.3×10^6 torr^{-1}s^{-1}), measured by the flowing afterglow technique, has been taken from [16]. The fairly good correlation between the quenching rates obtained in [3,4,16] is worth noticing.

After energy is transferred from the Kr($^1P_1$, $^3P_{1,2}$) states to excited states of XeI, radiative cascading populates the lower-lying states of XeI, eventually the Xe($^3P_1$, $^3P_2$) levels [1–5] (the role of the Xe($^1P_1$) and Xe($^3P_0$) states has not been published, as far as we know).

The rate of molecule-atom energy transfer from the krypton molecular 1_u state, resulting in direct excitation of the xenon atomic state $^3P_1$, was measured in [3] from the decay curves of the second krypton continuum at 145 nm (2×10^7 torr^{-1}s^{-1}). This high rate is in agreement with theoretical predictions [1,2] ($\sim 10^7$ torr^{-1}s^{-1}) and with estimates of the molecule-atom energy transfer cross-sections [1,2] made with a one order of magnitude uncertainty on the basis of spectroscopic experimental data ($\sim 10^{-13}$ cm^2 and $\sim 10^{-14}$ cm^2 for the $Kr_2^*(0_u^+)$ and $Kr_2^*(1_u)$ states respectively, that is $\sim 4 \times 10^8$ torr^{-1}s^{-1} and $\sim 4 \times 10^7$ torr^{-1}s^{-1}).

It should be pointed out that the products of two-body collisions of Kr($^3P_1$, $^3P_2$) atoms with ground-state Kr atoms usually have no definite identification in the cited literature and that there is a strong discrepancy between the measured values of the rate. We suppose that the mentioned process is, mainly, a two-body conversion of excited atoms in excited molecules.

One might consider energy transfer from krypton atoms and molecules to xenon atoms as the "first" stage of energy transfer in the kinetic model shown in Figure 12. For the lowest xenon concentrations used the result of this stage is the accumulation of excitation energy in the Xe($^3P_1$) level. This conclusion was made on the basis of the spectroscopic results [1–5] which, at the lowest Xe concentrations, showed, besides the Kr emissions, only the high intensity Xe emission at 147 nm. At low Xe concentrations, quenching of the Kr atomic states by Xe ground-state atoms is not as effective as the two- and three-body reactions with Kr atoms (Fig. 12), and the main channel of energy transfer is the molecule-atom channel. One may speculate that the assumption about a selective "initial" population of the Xe($^3P_1$) level is less valid for higher Xe concentrations when atom-atom energy transfer becomes equally or more efficient than molecule-atom energy transfer and the lowest Xe states are populated through radiative cascading (according to the data collected in Fig. 12, the two energy transfer channels become equally efficient when the Xe pressure reaches $P_{Xe} \cong 5 \times 10^{-6} P_{Kr}^2$). In this connection we can indicate the ratio between the Xe($^3P_1$) and Xe($^3P_2$) state populations after a cascade from the atomic Xe($6p$) states (Fig. 12), obtained in [29]: ~ 90 percent of the number of initially excited Xe($6p$) states decay through the Xe($^3P_1$) state and ~ 10 percent bypass to the Xe($^3P_2$) state. This branching ratio did not vary with pressure in the range 75–7500 torr [29]. Hence it might be reasonable to assume a strong population of the Xe($^3P_1$) state in our whole range of Xe pressures and therefore not take the "initial" population of the Xe($^3P_2$) state into account.

The next step of energy transfer is the depopulation of the Xe($^3P_1$) and Xe($^3P_2$) states. Direct measurements of collisional depopulation of the Xe($^3P_1$) state in Kr–Xe mixtures was performed only in [5] as far as we know. According to time-dependent intensity measurements of the xenon resonance line [5], the Xe($^3P_1$) state is depopulated by collisions with both Xe and Kr ground-state atoms. The rate $2100 P_{Kr}$ torr^{-1}s^{-1} was assigned to represent a collisional transition to the Xe($^3P_2$) metastable state. The rate $7 P_{Kr}^2$ torr^{-2}s^{-1} was assigned to represent the formation of $(KrXe)^*$ molecules, while the rate $97 P_{Xe} P_{Kr}$ torr^{-2}s^{-1} represents either the formation of the $Xe_2^*(0_u^+)$ states or $(XeKr)^*$ molecules. Unfortunately there is no direct information in [5] about the spectral resolution, so therefore we do not know whether the resonance line at $\lambda = 147.0$ nm was recorded together with or without the molecular structure around this line (Figs. 4–7).

The action of Kr ground-state atoms on the metastable Xe($^3P_2$) states was checked in [3] by carrying out a kinetic study of the 173 nm xenon second continuum. The two- and three-body rates of Xe($^3P_2$) state depopulation have been estimated, $3080 P_{Kr}$ torr^{-1}s^{-1} and $37 P_{Kr}^2$ torr^{-2}s^{-1},

Table 1. Parameters of the Morse potential curves presented in Figure 1 (see comments in Sect. 5). D_m is the depth of the potential well, R_m is the equilibrium internuclear distance, R_0 is the left zero value point of the Morse potential curve.

	KrXe						Xe_2		
	$1(^3P_1)$	$2(^3P_2)$	$0^+(^3P_1)$	$1(^3P_2)$	$0^-(^3P_2)$	$0^+(^1S_0)$	0^+_u	1_u	0^+_g
D_m, cm^{-1}	440 [13]	580 [11,13] *	920 [13]	1120 [11,13]	1230 [11]	159 [15]	4000 [21]	3500 [21]	196 [35]
R_m, Å	4.34 [11]	4.23 [11]	3.55 [13]	3.25 [13]	3.25 ***	4.18 [15]	3.2 [21]	3.2 [21]	4.36 [35]
R_0, Å	3.84 [11]	3.76 [11]	2.86 [13] **	2.65 [13]	2.65 [13]	3.7 [15]	2.5 [21]	2.5 [21]	3.89 [35] ****

* We used the ratio of the depths of the $1(^3P_1)$ and $2(^3P_2)$ states as in [11] and took D_m for the $1(^3P_1)$ state from [13].
** Slightly corrected (5.5 a_0 instead of 5 a_0) to get a crossing point between the $0^+(^3P_1)$ and $1(^3P_1)$ states as in [11] and [13].
*** We have taken the same R_m as for the $1(^3P_2)$ state (like in Fig. 3 in [11]).
**** The same value has been obtained from the absorption spectrum analysis in [37].

respectively. The authors did not indicate products of these reactions, however, so we believe that the mentioned processes are mainly two- and three-body conversion of excited atoms into excited Xe*Kr molecules.

Also the rate $(40 \pm 10)P_{Kr}P_{Xe}$ $torr^{-2}s^{-1}$ was derived in [3] from the decay of the 173 nm continuum, and was attributed to three-body formation of Xe_2^* molecules from $Xe(^3P_1)$ atoms. Notice that in [1,2] the formation of the Xe_2^* molecules was ascribed to three-body conversion of the $Xe(^3P_2)$ atoms.

It should be underlined that the scheme of processes indicated in Figure 12 does not include (for simplicity reasons) reactions with participation of electrons. In our case the electron density n_e is $\sim 10^{14}$ cm^{-3} [30]. Therefore, reactions having a rate $\sim n_e \times 10^{-9}$ s^{-1} or more should be taken into account. Collisions of excited atoms or molecules with electrons resulting in mixing of the level populations are most important in our case. If the separation in the energy between two levels is of the order of 1000 cm^{-1} or less, the mixing has the rate $\sim n_e \times 10^{-7}$ s^{-1} [31,32]. Therefore it is expected, for instance, that there is a strong mixing of the $^3P_1$ and $^3P_2$ atomic states in both Kr and Xe (Fig. 11) in the discharge channel.

From the results of [3,5] (Fig. 12) it follows that the mixed molecules Xe*Kr are the main product of depopulation of the $Xe(^3P_1, ^3P_2)$ states through collisions with atoms in any "krypton-small amount of xenon" mixture, at least at Xe concentrations $< 7\%$. The same conclusion could be drawn from general considerations; if the Kr/Xe concentration ratio is $> 100/1$ (as in our case), Xe atoms could compete with Kr in depopulation of the $Xe(^3P_1, ^3P_2)$ states only if they have a collisional cross section two orders of magnitude higher than Kr atoms which is unlikely. The aforesaid is in accordance with our spectra observed at Xe concentrations $< 0.1\%$. However, at Xe concentrations $> 0.1\%$, a total pressure ~ 300 torr and low gas temperature, the Xe_2^* continuum becomes the main feature of the VUV spectrum of the mixture (Figs. 9 and 10). Similar results were obtained at higher total pressures than in our discharges and at room temperature in [2,3]. The conclusion is that it is appropriate to look for an additional energy transfer processes.

The Morse potential curves for XeKr molecules (Fig. 1) will be used in the interpretation of the spectra depicted in Figures 3–10. These potential curves are derived from semiempirical calculations for the excited states [11,13] and data for the ground state presented in [15]. The restricted experimental results for the $1(^3P_1)$ state obtained in [8] were taken into account in the calculations [11–13]. For convenience, the Morse potentials of Xe_2 are also shown in Figure 1. The parameters used in the construction of the Morse potentials are presented in Table 1. For XeKr potentials we tried to use the data of [13] as the basic data but this publication contains the full sets of the Morse parameters only for the $0^+(^3P_1)$ and $1(^3P_2)$ states. Therefore it was necessary to combine the results of [11,13]. Sometimes the potential curves presented in [11,13] were used to derive a parameter. We consider the XeKr potentials shown in Figure 1 realistic but not very accurate.

A significant feature distinguishes the potential curves for Xe*Kr molecules from the curves for the Kr_2 or Xe_2 dimers, namely, according to the cited works [11–13], that there are "additional" bound excited electronic states. In reality, these are weakly bound states: the potential curves of the $1(^3P_1)$ and $2(^3P_2)$ states have shallow minima. These minima are situated at larger internuclear distances than the minima of the $0^+(^3P_1)$ and $1(^3P_2)$ states and at about the same internuclear distance as the weakly bound ground state $0^+(^1S_0)$. On the basis of the works [11,13] one can estimate the depths of the $1(^3P_1)$ and $2(^3P_2)$ wells to be some hundred cm^{-1}.

As underlined above, the atomic-molecular emission spectrum around $\lambda = 147.0$ nm (Figs. 4–6) is similar to the absorption spectrum of the Kr–Xe mixture close to the Xe resonance line (Fig. 7). This similarity indicates that both the emission and absorption spectra correspond to transitions between the same sets of upper and lower states. On the other hand, the structure of the Kr–Xe spectrum around the resonance line $\lambda = 147.0$ nm, that is the width and the presence of maxima and minima,

is quite different from that in pure Xe or Kr (see *e.g.* [33,34]). If we take the last two points into account, a comparison of the spectra (Figs. 4–7) with the potential curves (Fig. 1) indicates that molecular structure near $\lambda = 147.0$ nm, in absorption and in emission, is quite probably caused by transitions between the weakly bound ground state $0^+(^1S_0)$ and the weakly bound excited state $1(^3P_1)$.

The following remarks about the identification of the spectrum around $\lambda = 147.0$ nm can now be made. The depths of the $0^+(^1S_0)$ and $1(^3P_1)$ states are so small that each of them has a more or less uniform density distribution over the vibrational levels when it serves as the initial electronic state of the discussed transitions, and, consequently, the same set of molecular transitions and similar spectra may be observed in absorption and in emission. The width of the molecular spectrum from the resonance line at $\lambda = 147.0$ nm to the short wavelength side is ≈ 0.6 nm, corresponding to ≈ 300 cm^{-1} in energy. This value exceeds by a factor of 2 the depth of the ground state well (≈ 160 cm^{-1}) estimated in [35]. One may therefore conclude that the spectrum on the short wavelength side of $\lambda = 147.0$ nm partially originates from free-bound transitions between the repulsive part of the $1(^3P_1)$ state and the well of the $0^+(^1S_0)$ state. The presence of the very broad molecular bands on the short wavelength side in the range 146.3–146.8 nm [14] (part of them are seen in Fig. 5) supports this conclusion. We may also conclude that the minimum of the potential curve of the ground state $0^+(^1S_0)$ is situated at a larger internuclear distance than the minimum of the $1(^3P_1)$ state. The width of the molecular spectrum from the resonance line at $\lambda = 147.0$ nm to the long wavelength side indicates that the well depths of the $1(^3P_1)$ and $0^+(^1S_0)$ states should be about the same. These facts are the starting points for the identification of the spectrum around $\lambda = 147.0$ nm. The previous analysis has shown that all details of the spectrum, including the strong peak on the long wavelength side (which was assigned as the atomic line wing in [14,15], can be considered as transitions between vibrational levels of the $1(^3P_1)$ and $0^+(^1S_0)$ states.

It is now possible to interpret the spectra in Figures 3, 8–10 and, in particular, give an explanation of the appearance of the Xe_2 continuum. At low xenon concentrations, the emissions related to the xenon admixture concentrate around the xenon resonance line $\lambda = 146.97$ nm (Figs. 3–6). The long wavelength low intensity "non-krypton" continuum, originating from transitions in Xe*Kr molecules from the lower vibrational levels of the $0^+(^3P_1)$ or $1(^3P_2)$ states, becomes distinguishable only at Xe concentrations $\approx 0.1\%$ (Fig. 3). If the total pressure is low enough, the integral intensity of the band around $\lambda = 147.0$ nm exceeds significantly the integral intensity of the mixed molecule continuum from the strongly bound states. For instance, at a total pressure of 100 torr and 0.1% Xe admixture, the ratio of the two intensities is about 10 according to our spectra. Making this estimate, we did not take self-absorption in the band into account. In reality the ratio is higher. The aforesaid indicates, firstly, a high population of the $1(^3P_1)$ mixed molecule state, and, secondly, that the band around $\lambda = 147.0$ nm is the main channel of radiative losses of the mixed molecules.

When the Xe concentration or the total pressure increases, the ratio between the integral intensity in the band around $\lambda = 147.0$ nm and the intensity of the mixed molecule continuum goes down. Partially this can be connected with a more rapid growth of the continuum intensity than of the band intensity, but the main reason is growing self-absorption in the band around $\lambda = 147.0$ nm since the detection of the light with the spectrometer is done along the discharge capillary and through the gas layer between the discharge channel and the exit window. Therefore, the decreasing ratio of the integral intensities observed in the spectra does not mean that the main part of the Xe*Kr emission from the emitting volume begins to concentrate in the continuum. One should remember that with a long and narrow emitting volume as in our case, the radiative losses that are not along the capillary but in the lateral direction are most important. It is obvious that the relative intensity of the band around $\lambda = 147.0$ nm is much higher at the inner capillary wall than what we obtain in the spectra observed along the capillary. Consequently, the band around $\lambda = 147.0$ nm is not so strongly trapped in the uncooled capillary as it seems from the spectra observed along the capillary.

This conclusion is also confirmed by the following: the spectra in Figures 3 and 8 and the spectra 1, 2 in Figure 9 show a significant difference between the integral intensity of the Kr–Xe mixture spectrum and the integral intensity of the pure Kr spectrum. But, in accordance with the scheme of the processes (Fig. 12), these integral intensities should not differ significantly because energy, transferred from the Kr molecules to the Xe atoms and, further, to the mixed molecules, should be emitted in the VUV range indicated in the figures.

Cooling of the capillary walls with liquid nitrogen vapours increases the gas density in the capillary and, what is more important in our case, increases the concentration of the XeKr ground state molecules, especially near the inner capillary wall. A well-known formula of statistical mechanics was used in [32] for estimates of the molecular concentrations in weakly bound ground states. For the XeKr mixture this formula gives, at a total pressure of 300 torr, 1% of Xe and a gas temperature of 110 K, a relative density ratio $N_m/N_a \approx 3\%$, where N_m and N_a are the concentrations of ground state XeKr molecules and Xe atoms respectively. However, since the condensed phase should be taken into account, this could be an underestimate when the gas temperature approaches the temperature of gas condensation and the density of the weakly bound molecule grows much more rapidly than the formula predicts. A growth of the XeKr molecule density leads to increasing self-absorption and trapping of the band around $\lambda = 147.0$ nm emitted in the lateral direction. Consequently, the efficient lifetime of the Xe*Kr $1(^3P_1)$ state increases and the probability of excitation transfer from the Xe*Kr $1(^3P_1)$ state grows.

The spectra in Figures 9 and 10 indicate that excitation energy is transferred to the Xe*Kr states and to the

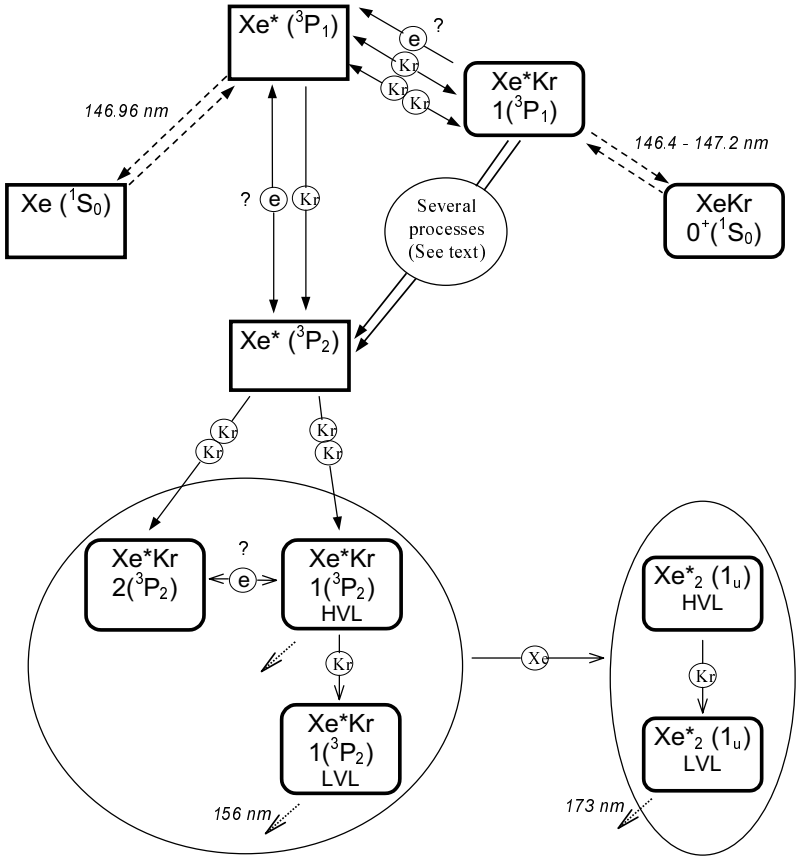

Fig. 13. Simplified scheme of energy transfer processes in a "krypton-small amount of xenon" mixture, in accordance with the results of this work (see details and comments in text). It is supposed that "initially", after energy transfer from Kr to Xe, excitation is mainly concentrated in the Xe*(^{3}P$_1$) state (see Fig. 12). Reactions of atomic and molecular state mixing by electrons are marked by the sign "?" because it is assumed that energy transfer processes take place not only in but also outside the discharge channel. HVL (LVL) means high (low) vibrational levels.

Xe_2^* states emitting the continua with maxima at 156 nm and 173 nm. One should remember that Xe_2^* molecules, as has been supposed above, will not appear as a result of a three-body conversion of the excited Xe atoms in competition with three-body conversion to mixed molecules.

According to our analysis of the spectra, the trapping of the band around $\lambda = 147$ nm leads to an increase of excitation transfer to the Xe*(^{3}P$_2$) state (Fig. 13). A number of processes may contribute. Firstly, an increasing efficient lifetime of the Xe*Kr 1(^{3}P$_1$) state will lead to an increase of the efficient lifetime of the atomic precursor, Xe*(^{3}P$_1$). In this case, mixing of the Xe*(^{3}P$_1$) and Xe*(^{3}P$_2$) states assisted by collisions with electrons and atoms gives a higher efficiency of excitation transfer to the Xe*(^{3}P$_2$) state in a cooled capillary than in an uncooled capillary.

Secondly, the trapping of the band around $\lambda = 147.0$ nm leads to a growth of excitation transfer to the Xe*Kr(0$^+$(^{3}P$_1$)) molecule *via* mixing of the 1(^{3}P$_1$) and 0$^+$(^{3}P$_1$) states (see Fig. 1) by electrons, and/or can initiate the following two reactions:

$$\mathrm{Xe^*Kr}(1(^3\mathrm{P}_1),\, 0^+(^3\mathrm{P}_1)) + \mathrm{Xe}(^1\mathrm{S}_0) \rightarrow \mathrm{Xe}_2^*(0_u^+) + \mathrm{Kr}(^1\mathrm{S}_0). \quad (1)$$

The $Xe_2^*(0_u^+)$ and Xe*Kr(0$^+$(^{3}P$_1$)) molecules can be formed only in the upper vibrational states and therefore, to emit the second continua at 156 nm and 173 nm, they must relax (in collisions with the atoms) to their lowest vibrational levels. The natural lifetimes of these upper vibrational levels are very short (nanoseconds) which raises the question if relaxation to the lowest vibrational levels is possible at our total pressures. In this connection we refer to results reported in [29] where the observation of the temporal behaviour of the second Xe_2^* continuum was carried out in pure Xe. It was shown that a contribution of the $Xe_2^*(0_u^+)$ state to the second continuum shows up at Xe concentrations $> 4 \times 10^{19}$ cm^{-3}. This result is not in full agreement with the vibrational relaxation rate for the $Xe_2^*(0_u^+)$ state, 7×10^{-11} cm^{3}s^{-1}, obtained in [36]. We therefore believe that the latter value of the relaxation rate is too high since relaxation from the highest vibrational levels was not investigated in [36]. We have derived an estimate for this rate from the results of [29] to be $< 10^{-11}$ cm^{3}s^{-1}. Another result obtained in [36], the rate for $Xe_2^*(0_u^+)$ vibrational relaxation in collisions with Ar, is 6×10^{-12} cm^{3}s^{-1} which indicates an upper limit of the rate for $Xe_2^*(0_u^+)$ vibrational relaxation in collisions with Kr. In [6] relaxation constants of Xe_2^* and Xe*Kr molecules with krypton as a buffer gas were estimated to be 2×10^{-12} cm^{3}s^{-1} for both excimer systems. The listed results give reasons to believe that, at the total pressures used in our experiments, the relaxation from the upper to the lowest vibrational levels of both the $Xe_2^*(0_u^+)$ and Xe*Kr(0$^+$(^{3}P$_1$)) molecular states is unlikely.

In accordance with [29], one can assume that the main part of the $Xe_2^*(0_u^+)$ molecules, being in their upper vibrational levels, dissociate along the repulsive potential

curves forming the two atomic $Xe^*(^3P_2)$ and $Xe(^1S_0)$ states (the single repulsive curve shown in Fig. 1 symbolises the $1g$, $0g^-$, and $2u$ repulsive states). The ratio 0.29 between the relaxation and dissociation rates was obtained in [29]. According to our estimates derived from the results of [29], the dissociation rate for the $Xe_2^*(0_u^+)$ molecule is $\approx 3 \times 10^{-11}$ cm^{3}s^{-1}. The same type of dissociation of the $Xe^*Kr(0^+(^3P_1))$ molecules can occur *via* the $Xe^*Kr(2(^3P_2))$ weakly bound state.

Hence, the growing trapping of the band around $\lambda = 147.0$ nm leads, in different ways, to an increase of excitation transfer to the $Xe^*(^3P_2)$ state. The $Xe^*(^3P_2)$ atoms, appearing as a result of a dissociation or a mixing, are then converted in a three-body process into $Xe^*(^3P_2)Kr$ molecules, which have longer (approximately one order of magnitude) radiative lifetimes than $Xe^*(^3P_1)Kr$ molecules. By analogy with conversion of the $Xe^*(^3P_1)$ state, one can assume that a significant part of the $Xe^*(^3P_2)$ atoms will be converted into weakly bound $Xe^*Kr(2(^3P_2))$ molecules (the optical transitions from the $2(^3P_2)$ state to the ground state are forbidden). Therefore, the two reactions

$$Xe^*Kr(1(^3P_2), 2(^3P_2)) + Xe(^1S_0) \rightarrow Xe_2^*(1_u) + Kr(^1S_0) \quad (2)$$

can be efficient. A total pressure of 300 torr is undoubtedly enough for collisional relaxation of both $Xe^*Kr(1(^3P_2))$ and $Xe_2^*(1_u)$ molecules to the lowest vibrational levels and the subsequent emission of the continua around 156 nm and 173 nm.

If we apply the aforesaid to an interpretation of the spectra 2, 3 and 4 in Figure 9, we conclude, first of all, that the growth of the total intensity of the continuous emission of the mixture with cooling is a result of trapping of the band around $\lambda = 147.0$ nm emitted in the direction to the capillary wall. Secondly, the intensity of the continuum at 173 nm grows faster than that at 156 nm because the Xe concentration increases under cooling and the efficiency of the reactions (2) grows. Thirdly, one may draw the conclusion from spectra 2, 3, 4 that the rate of the reaction (2) is of the same order of magnitude as the radiative decay of the mixed molecules taking part in the reaction. Figure 10 shows that a certain level of Xe concentration is necessary to obtain "the effect of cooling" (spectra 3 and 4 in comparison with spectrum 2). Firstly, the Xe concentration should be high enough for effective trapping of the band around $\lambda = 147.0$ nm. Secondly, the Xe concentration should also be high enough for a successful competition with the radiative decay of the $Xe^*Kr(2(^3P_2))$ molecules.

As a summary of this chapter, we want to make the following remarks.

- As mentioned above, a spectrum similar to the spectrum 4 in Figure 9 was observed in [2,3] at room temperature and total pressures of 1000 torr [2] and 500 torr [3] when the xenon concentration increased up to 2.5% and 1%, respectively. The lateral dimensions of the cells used for excitation of the mixture in [2,3] were $\leq$ 1 cm and 10 cm, respectively. That is: higher total pressure and Xe concentration are necessary to observe the Xe_2^* continuum at 173 nm in cells with small dimensions. One might suppose that the results from [2,3] confirm that the effect of trapping of the emission in the band around $\lambda = 147.0$ nm plays an important role for the interpretation of our results.
- The intensity of the Kr_2 continuum grows under cooling (spectrum 1 in Fig. 10 and spectrum 1 in Fig. 9). This effect was investigated in [32]. It should be pointed out that the integral intensity of the Kr–Xe spectrum under cooling (spectrum 4 in Fig. 10) is higher than the intensity of the Kr_2 continuum (spectrum 1 in Fig. 10). To understand this, we have to take into account that excitation is transferred from Kr to Xe through two channels, the "molecule-atom" channel as well as the "atom-atom" channel. The difference in the intensities can be connected with the growth of the "atom-atom" channel contribution at higher Xe pressures.
- In reality it is not possible to separate the emission from the $Xe^*Kr(1(^3P_1))$ molecules and from the uppermost vibrational levels of the $Xe^*Kr(0^+(^3P_1))$ state. When talking about $Xe^*Kr(1(^3P_1))$ emission, we also mean emission from the uppermost vibrational levels of the $Xe^*Kr(0^+(^3P_1))$ state.
- In this work a contracted discharge was used, having a narrow diameter ($\approx$ 0.5 mm) discharge channel along the axis of the discharge capillary. The molecular self-absorption and trapping of the band around $\lambda = 147.0$ nm takes place mainly in cold layers close to the inner capillary wall. A growth of the trapping with cooling leads to a consequent increase of the concentration of excited molecules (and atoms) in these layers. This in turn means that the processes of energy transfer described above and, consequently, also the emission of the continua may occur predominantly near the inner capillary wall, that is outside the discharge channel.
- Only the "main route" of excitation transfer from the trapped $Xe^*(^3P_1)$ state has been discussed in this paper. A simplified scheme of energy transfer processes starting from the $Xe^*(^3P_1)$ state is shown in Figure 13.

A number of observations remain to be interpreted. In particular, a rather intense structure of molecular origin has been observed near the Kr resonance lines. Possibly, Kr*Xe molecules can also be the starting point of energy transfer from Kr to Xe.

4 Conclusion

The results of the work extend the understanding of the mixed molecule role in generating the VUV spectrum from a mixture of "krypton-small amount of xenon". The creation of excited mixed molecules Xe*Kr is the basic channel of energy transfer from the atomic xenon state $Xe^*(^3P_1)$ which is a result of energy transfer from krypton to xenon. A strong emission peak from a weakly bound

excited Xe^*Kr state is observed around $\lambda = 147.0$ nm together with continuous emission from a more strongly bound excited Xe^*Kr state. Mixed molecule emission determines the spectrum of the mixture until emission in the band around $\lambda = 147$ nm becomes strongly limited by self-absorption. In our case this occurs when the discharge capillary wall is cooled down to temperatures close to the temperature of gas condensation. With cooling, the $Xe_2^*(1_u)$ molecule emission becomes the main feature of the spectrum. However, the mixed molecules work as an important link in the energy transfer processes, even when their contribution to the spectrum is small.

This work was supported by the Swedish Research Council for Engineering Sciences (TFR) and by Carl Tryggers Stiftelse for Vetenskaplig Forskning. Two of us, B.K. and G.G., would like to thank the Department of Physics, Uppsala University, for its hospitality. We also thank Dr. Alexei Utkin at the Department of Computational Physics, St. Petersburg State University, for the software used in our data acquisition system.

References

1. A. Gedanken, J. Jortner, B. Raz, A. Szoke, J. Chem. Phys. **57**, 3456 (1972).
2. O. Cheshnovsky, B. Raz, J. Jortner, J. Chem. Phys. **59**, 3301 (1973).
3. Y. Salamero, A. Birot, H. Brunet, H. Dijols, J. Galy, P. Millet, J.P. Montagne, J. Chem. Phys. **74**, 288 (1981).
4. J.D. Cook, P.K. Leichner, Phys. Rev. A **31**, 90 (1985).
5. J.D. Cook, P.K. Leichner, Phys. Rev. A **43**, 1614 (1991).
6. N.A. Kryukov, M.A. Chaplygin, Opt. Spectrosc. **82**, 510 (1997).
7. E.T. Verkhovtseva, A.E. Ovechkin, Opt. Spectrosc. **47**, 117 (1979).
8. G. Nowak, J. Fricke, J. Phys. B: At. Mol. Phys. **18**, 1355 (1985).
9. A.G. Belov, A.D. Klementov, S.A. Pendyur, I.Ya. Fugol, E.M. Yurtaeva, Opt. Spectrosc. **61**, 601 (1986).
10. P. Laporte, P. Gurtler, E. Morikawa, R. Reininger, V. Saile, Europhys. Lett. **9**, 533 (1989).
11. A.L. Zagrebin, N.A. Pavlovskaya, Opt. Spectrosc. **69**, 320 (1990).
12. A.Z. Devdariani, A.L. Zagrebin, Opt. Spectrosc. **72**, 309 (1992).
13. A.L. Zagrebin, S.I. Tserkovnyi, Chem. Phys. Lett. **239**, 136 (1995).
14. D.E. Freeman, K. Yoshino, Y. Tanaka, J. Chem. Phys. **67**, 3462 (1977).
15. M.C. Castex, J. Chem. Phys. **66**, 3854 (1977).
16. J.E. Velazco J.H. Kolts, D.W. Setser, J. Chem. Phys. **69**, 4357 (1978).
17. R. Turner, Phys. Rev. **158**, 121 (1967).
18. Y. Salamero, A. Birot, H. Brunet, J. Galy, P. Millet, J. Chem. Phys. **80**, 4774 (1984).
19. P.R. Timpson, J.M. Anderson, Can. J. Phys. **70**, 380 (1979).
20. W. Wieme, M. Vanmarcke, Phys. Lett. A **72**, 215 (1979).
21. Y. Salamero, A. Birot, H. Brunet, J.N. Foulquier, J. Galy, P. Millet, M. Rouzaud, J.L. Teyssier, J. Phys. B: At. Mol. Opt. Phys. **21**, 2015 (1988).
22. P.K. Leichner, R.J. Ericson, Phys. Rev. A **9**, 251 (1974).
23. R. Boucique, P. Mortier, J. Phys. D: Appl. Phys. **3**, 1905 (1970).
24. T. Oka, K.V.S. Rama Rao, J.L. Redpath, R.F. Firestone, J. Chem. Phys. **61**, 4740 (1974).
25. J.W. Keto, R.E. Gleason, T.D. Bonifield, G.K. Walters, F.K. Soley, Chem. Phys. Lett. **42**, 125 (1976).
26. Y. Salamero, A. Birot, H. Brunet, J. Galy, P. Millet, J.P. Montagne, J. Phys. B: At. Mol. Opt. Phys. **12**, 419 (1979).
27. A.V. Phelps, Phys. Rev. **114**, 1011 (1958).
28. R. Turner, Phys. Rev. **140**, A426 (1965).
29. P. Moutard, P. Laporte, J.-L. Subtil, N. Damany, H. Damany, J. Chem. Phys. **88**, 7485 (1988).
30. G. Gerasimov, B. Krylov, G. Zvereva, R. Hallin, A. Arnesen, F. Heijkenskjold, Opt. Spectrosc. **81**, 857 (1996).
31. C.W. Werner, E.V. George, P.W. Hoff, C.K. Rhodes, IEEE J. Quantum Electrn. **QE-13**, 769 (1977).
32. G. Gerasimov, B. Krylov, A. Loginov, G. Zvereva, R. Hallin, A. Arnesen, F. Heijkenskjold, Appl. Phys. B **66**, 81 (1998).
33. R.E. Huffman, J.C. Larrabee, Y. Tanaka, Appl. Opt. **4**, 1581 (1965).
34. Y. Tanaka, K. Yoshino, D.E. Freeman, J. Chem. Phys. **59**, 5160 (1973).
35. M.V. Bobetic, J.A. Barker, J. Chem. Phys. **64**, 2367 (1976).
36. T.D. Bonifield, F.H.K. Rambow, G.K. Walters, M.V. McCusker, D.C. Lorents, R.A. Gutcheck, J. Chem. Phys. **72**, 2914 (1980).
37. M.-C. Castex, J. Chem. Phys. **74**, 759 (1981).